Three-Dimensional Subwavelength Imaging by a Photonic-Crystal Flat Lens Using Negative Refraction at Microwave Frequencies

Zhaolin Lu, Janusz A. Murakowski, Christopher A. Schuetz, Shouyuan Shi, Garrett J. Schneider, and Dennis W. Prather

Department of Electrical and Computer Engineering, University of Delaware, Newark, Delaware 19716, USA

(Received 23 March 2005; published 4 October 2005)

We experimentally demonstrate subwavelength resolution imaging at microwave frequencies by a three-dimensional (3D) photonic-crystal flat lens using full 3D negative refraction. The photonic crystal was fabricated in a layer-by-layer process. A subwavelength pinhole source and a dipole detector were employed for the measurement. By point-by-point scanning, we obtained the image of the pinhole source shown in both amplitude and phase, which demonstrated the imaging mechanism and subwavelength feature size in all three dimensions. An image of two pinhole sources with subwavelength spacing showed two resolved spots, which further verified subwavelength resolution.

DOI: 10.1103/PhysRevLett.95.153901 PACS numbers: 42.70.Qs, 42.25.Gy, 42.30.−d, 78.20.−e

Recent interest in negative refraction has motivated the study of imaging by a flat lens, which offers the possibility of creating a ''perfect lens'' as proposed by Pendry [1]. His theoretical work showed that negative refraction amplifies evanescent waves, which in turn contributes to a higher resolution image. The end result is a lens with a resolution not limited by working wavelength. However, Pendry's claim sparked many debates concerning the basis of negative refraction and the corresponding flat lens. While some of these debates focused on whether negative refraction is possible and how it would function [2–5], others focused on whether negative refraction could make a ''perfect lens'' [6–8]. In any case, vast interest in imaging by negative refraction has arisen in materials science, radio frequency engineering, electrical engineering, optical communication, optical storage, and medical engineering. Parimi *et al.* demonstrated imaging by a planar photonic-crystal (PhC) flat lens using negative refraction [9,10]. Recently, we demonstrated negative refraction imaging of a millimeter-wave dipole in both amplitude and phase by a ''flat cylindrical'' lens composed of either a square-lattice [11] or a triangular-lattice [12] photonic crystal. While 2D flat lenses constitute important breakthroughs for investigating negative refraction and super resolution lenses, they are seldom used in real optical systems since these 2D photonic flat lenses have lensing ability only along one direction, which correspond to conventional planar lenses [9,10] or cylindrical lenses [11,12] and have severe limitations for realistic applications. Strictly speaking, they are not fully functional lenses yet. Instead, most applications require the use of spherical lenses. For this reason, ''flat spherical'' lenses, which work by full 3D negative refraction (F3DNR) and provide super resolution imaging, are especially desired. The realization of such lenses is not only important for many applications, but also significant for fundamental research since F3DNR is a basic physical phenomenon that until now has never been experimentally demonstrated. In addition, previously demonstrated 2D negative refraction did not dispel various doubts on the existence of negative refraction [2–5] because in the 2D demonstrations either severe confinement (e.g., planar PhC flat lenses) is required or negative refraction is only partially observed (e.g., $k_z = 0$ for flat cylindrical lenses). Thus, the demonstration of a lens providing super resolution images based on F3DNR is a much more direct confirmation of the existence of negative refraction. Herein we present the first experimental demonstration of a lens based on F3DNR and its subwavelength resolution imaging.

Luo *et al.* [13] and Ao *et al.* [14] proposed and theoretically investigated such lenses, which are made of 3D PhCs. However, experimental demonstration of such lenses has never been reported since the fabrication of 3D PhCs is still very difficult, and engineering PhCs with such anomalous dispersion, F3DNR, is even more challenging. In the present work, we have overcome these challenges and succeeded in fabricating such a lens. Our experiments not only demonstrate imaging using F3DNR, but also verify its subwavelength resolution.

We used a body-centered cubic (bcc) structure similar to one proposed by Luo *et al.* [13]. A low-loss dielectric material, HiK 500 F from Emerson & Cuming, with $\varepsilon_r = 25$ at microwave frequencies was employed. The unit cell of our structure is shown in Fig. 1(a). The period of the bcc lattice as fabricated is $a = 6.35$ mm. There is one air cube with side $b = (3/4)a$ at each corner and at the center of a conventional cubic cell. Since $2b > a$, these nine air cubes overlap each other. This cubic cell has high symmetry, but is not easy to fabricate directly. However, if we shift by $(3/8)a$ along the lattice in vertical direction, we obtain an alterative cubic cell as shown in Fig. 1(b), which can be fabricated in two steps: (1) pattern one $(3/4)a \times (3/4)a \times (1/4)a$ air cube at the center and one $(3/4)a \times (3/4)a \times (3/4)a$ air cube at each corner on a slab with thickness a; (2) flip the slab and pattern the bottom air cube with dimensions, $(3/4)a \times (3/4)a \times (1/2)a$. Following this

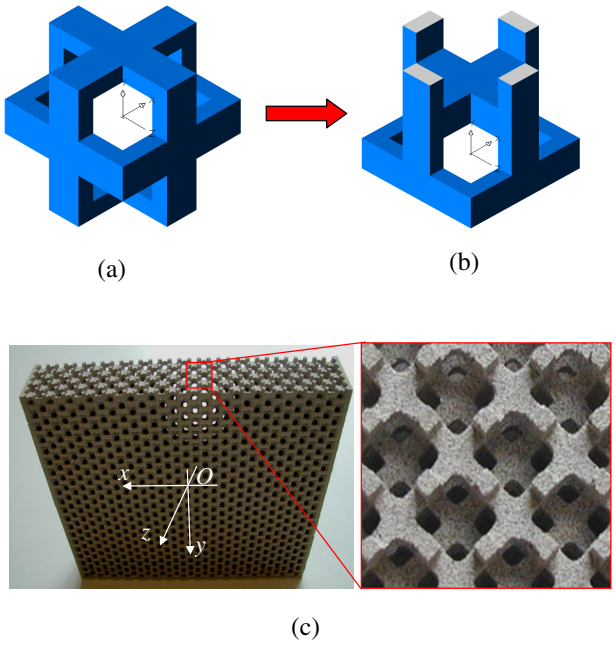

FIG. 1 (color online). (a) Conventional cubic unit cell of the bcc structure. (b) The modified unit cell after shifting by $(3/8)a$ along vertical direction. (c) Three-dimensional PhC fabricated layer by layer (20 layers in total).

process and using a computer numerically controlled micro-milling machine, we fabricated the bcc PhC with 20 layers along the vertical direction, as shown in Fig. 1(c). Note that the (101) plane is the flat lens surface, so the lattice orientation has been rotated 45° around the vertical axis. The size of the lens is 25 mm (thickness) × 140 mm (width) × 127 mm (height).

By applying the plane-wave expansion method to Maxwell's equations, we solved for the eigenfrequencies at a given wave vector [15] and obtained results very similar to those of Luo *et al.* [13]. Figure 2(a) shows the band structure of our PhC. The tilted black straight lines in Fig. 2(a) represent the dispersion curve for air, namely, light lines. Group velocity is calculated as the gradient of the frequency in k space, i.e., $\mathbf{v}_g = \nabla_k \omega$. Dispersion curves

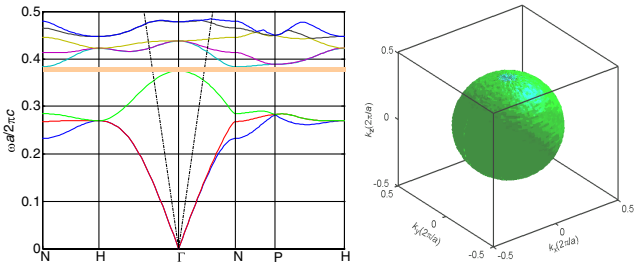

FIG. 2 (color online). (a) Band structure of the bcc lattice photonic crystal. (b) The constant-frequency surface of the crystal at $f = 0.36(c/a)$ (or 17.0 GHz for our structure) in the first Brillouin zone.

of regular materials have a group velocity with a positive radial component, resulting in $\mathbf{k} \cdot \mathbf{v}_g > 0$. However, the dispersion curve at the top of the third band of our PhC shows frequency increases with $|\mathbf{k}|$ decreasing, resulting in $\mathbf{k} \cdot \mathbf{v}_g < 0$. In other words, phase velocity is opposite to group velocity for a given electromagnetic wave as it propagates in the 3D PhC within this frequency range. The result is negative refraction. As shown in Fig. 2(b), the constant-frequency surface for a frequency in this range is nearly spherical, which makes F3DNR possible. However, compared with the results of Luo *et al.*, each of the corresponding frequencies in our dispersion diagram is lower due to the use of higher dielectric constant $\varepsilon_r = 25$, as opposed to $\varepsilon_r = 18$. As a result, F3DNR is expected to occur at frequencies $0.33c/a$–$0.36c/a$ (c is the speed of light in vacuum), or 15.6–17.0 GHz. In particular, we pay close attention to the frequency where the dispersion curve crosses the light line, $f = 17.0$ GHz in our case, because $n_{\text{eff}} = -1$ is expected at that frequency, which is important to minimize aberrations. Otherwise, at the third band, $|n_{\text{eff}}| > 1$ for 15.6 GHz $< f <$ 17.0 GHz, while $|n_{\text{eff}}| < 1$ for 17.0 GHz $< f <$ 17.8 GHz [16]. In addition, a small band gap appears between the third and the fourth bands, but that is not a precondition for negative refraction.

To form a point source, we took a 5 mm thick low-density foam board, covered its one side with aluminum foil, punched a 3 mm diameter pinhole through the foil at the center, attached the foam board to the flat lens with the foil facing away from the lens, and the pinhole aligned with the center of the flat surface, and illuminated the pinhole with a horn antenna. As a result, a quite symmetric point source is obtained according to Huygen's principle, although most of the waves emanating from it are evanescent because the pinhole is so small compared with the wavelength. The distance between the source and surface of the lens is determined by the thickness of the foam board, i.e., $d_0 = 5$ mm in our case. The dielectric constant of the foam board material is ~1 at the frequency of interest, so it has negligible effect on the electromagnetic wave propagation.

To test the performance of the lens, we built a microwave imaging setup based on an Agilent 85106D vector network analyzer. For the detector, we used a section of a 50 Ohm coaxial cable, 1.8 mm (0.07 in) in diameter, with a 1 mm length of core exposed at the end; the orientation of the detector, which senses electric field, coincides with the polarization (along the x axis) of the incoming wave [17]. The detector is mounted on an XYZ scanner to map the electric field. The PhC flat lens is placed on a Teflon bar, which has low dielectric constant. We scanned a 3D field distribution in the image space point by point with pixel size 2 mm × 2 mm × 2 mm, and total volume 100 mm × 100 mm × 50 mm. Meanwhile, the frequencies spanned the range from 12 to 20 GHz with spacing 0.2 GHz. As a consequence, we were able to capture 3D images of the

pinhole source in both amplitude and phase. We found good 3D images at $z = 11$ mm for sources with frequencies 16.0–17.2 GHz. It is seen that the electromagnetic waves converge first, and then diverge into the far field, which precludes the possibility that the subwavelength image is observed because the detector is very close to the source. Once the frequency range and image position were experimentally determined, we performed a dense scan (with pixel size 1 mm $\times$ 1 mm) at $z = 11$ mm in the frequency range 15.5–17.5 GHz with spacing 0.1 GHz. Figure 3 shows the image (intensity) obtained at $f = 16.4$ GHz ($\lambda = 18.3$ mm). According to this intensity distribution, the image size is found to be 7 mm(x) $\times$ 6 mm(y) by full width at half maximum (FWHM), which averages 6.5 mm, i.e., 36% of the vacuum wavelength. Therefore, the experiment successfully validates subwavelength-feature-size imaging by the 3D PhC flat lens. The increased size of the image as compared to the size of the source (6.5 mm vs 3.0 mm) can be understood if the periodicity of the photonic crystals is taken into consideration. According to Ref. [8], the photonic crystal imposes an upper cutoff to the wave vector of the evanescent waves that can be amplified. This cutoff provides the lower bound on the image size, which in our case approaches the periodicity of the photonic crystal used for the lens just as predicted in Ref. [8].

The distance of the image from the lens is different than expected from a simple effective-index theory where the distance between the source and its image is equal to twice the lens thickness for $n_{\text{eff}} = -1$. The discrepancy is most likely the result of the structure of the lens material and its boundary. In particular, it appears that the physical thickness of the lens, 25 mm, is larger than its effective thickness, i.e., the thickness seen by the electromagnetic wave [18]. According to this interpretation, the experimental results indicate that the effective lens thickness is about 20.5 mm, or, in other words, the lens effective boundary is shifted by about 2.25 mm inside the material.

To see the image formation more clearly, we found the image center in Fig. 3 and scanned the image space through the image center along the vertical plane yz and along the horizontal plane xz, separately. Figs. 4(a) and 4(b) show the intensity and phase distributions obtained from these scans at $f = 16.4$ GHz, and also include the side and top views of the PhC lens located between the source and the image. The high intensity spot along with the closed phase circle on either vertical plane or horizontal plane indicates how the image is formed. Furthermore, the FWHM in the vertical (yz) plane is measured to be 7 mm(y) $\times$ 9 mm(z), while that in horizontal (xz) plane, 8 mm(x) $\times$ 9 mm(z), which implies subwavelength feature size in all three dimensions. Since most of the waves from the source are evanescent, our result also verified that the image is formed by the amplification of evanescent waves [19].

To further validate subwavelength resolution, we introduced another pinhole with the same diameter and 10 mm (0.55λ, $\lambda = 18.3$ mm) away from the first one and repeated the scanning in vertical plane at $z = 11$ mm. Figure 5(a) shows the image we obtained at that plane. The resulting image shows two clearly resolved spots 10 mm apart, which corresponds to 0.55λ. Ten-millimeter separation in object space corresponds to 10 mm separation in image space. Therefore, the magnification of the system is 1, which is expected because the lens is flat and has translation symmetry in the xy plane. Further analysis of this image indicates that the resolution is potentially 2 mm better than that number [Fig. 5(b)], i.e., point sources 8 mm apart should be resolvable.

In conclusion, a 3D PhC flat lens was fabricated, and a series of experiments on it demonstrated F3DNR imaging of a point source in both amplitude and phase. The analysis of the acquired field distribution verified for the first time

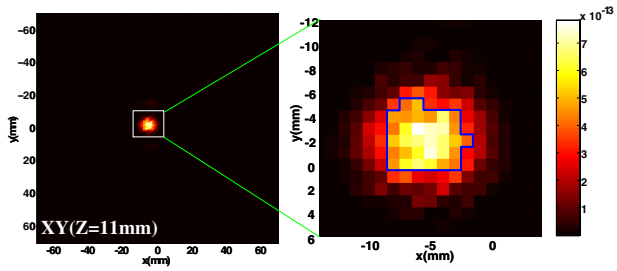

FIG. 3 (color online). Image of the point source achieved through the 3D PhC flat lens at image distance $d_i = 11$ mm. The enclosed block shows the dimensions of the spot size measured by FWHM.

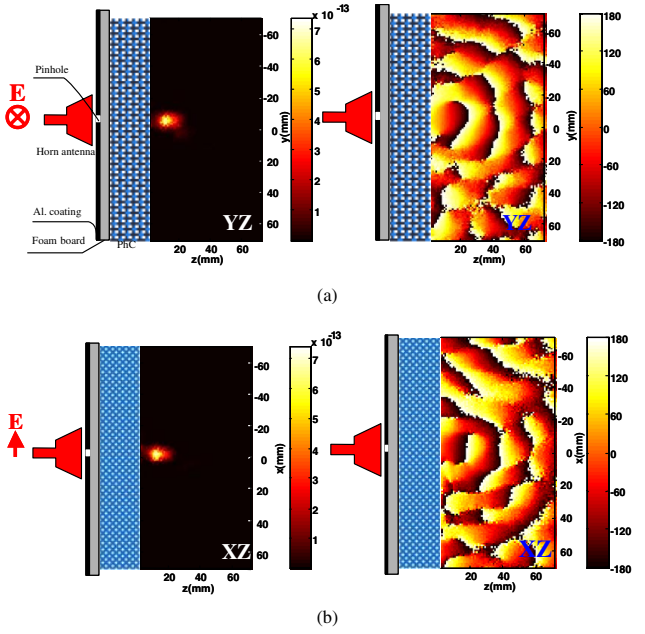

FIG. 4 (color online). Measured intensity and phase distributions ($f = 16.4$ GHz, $\lambda = 18.3$ mm): (a) in the vertical plane, (b) in the horizontal plane.

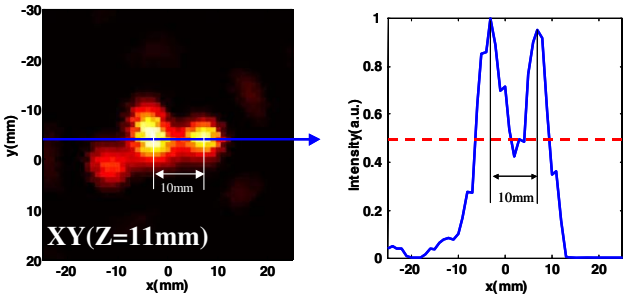

(a) (b)

FIG. 5 (color online). (a) The image (intensity) of two pinholes 10 mm apart ($\lambda = 18.3$ mm). (b) The intensity distribution along the blue line marked on (a). The image shows two resolvable spots with distance 10 mm.

3D subwavelength imaging using F3DNR. The image of two pinhole sources with subwavelength spacing showed two resolvable spots, which served to further validate subwavelength resolution. To some extent, this is the first time that a fully functional negative refraction material has been fabricated and characterized. These results have both theoretical and experimental significance and constitute a breakthrough toward the development of novel materials and 3D functional perfect lenses.

We would like to acknowledge the support of Dr. Gernot Pomrenke from the Air Force Office of Scientific Research (AFOSR) and Dr. Jim King from the Office of Naval Research.

[1] J. B. Pendry, Phys. Rev. Lett. **85**, 3966 (2000).
[2] P. M. Valanju, R. M. Walser, and A. P. Valanju, Phys. Rev. Lett. **88**, 187401 (2002).
[3] N. Garcia and M. Nieto-Vesperinas, Opt. Lett. **27**, 885 (2002).
[4] D. R. Smith, D. Schurig, and J. B. Pendry, Appl. Phys. Lett. **81**, 2713 (2002).
[5] J. B. Pendry, Nature (London) **423**, 22 (2003).
[6] N. Garcia1 and M. Nieto-Vesperinas, Phys. Rev. Lett. **88**, 207403 (2002).
[7] L. Venema, Nature (London) **420**, 119 (2002).
[8] C. Luo, S. G. Johnson, J. D. Joannopoulos, and J. B. Pendry, Phys. Rev. B **68**, 045115 (2003).
[9] P. V. Parimi, W. T. Lu, P. Vodo, J. Sokoloff, J. S. Derov, and S. Sridhar, Phys. Rev. Lett. **92**, 127401 (2004).
[10] P. V. Parimi, W. T. Lu, P. Vodo, and S. Sridhar, Nature (London) **426**, 404 (2003).
[11] Z. Lu, S. Shi, C. A. Schuetz, and D. W. Prather, Opt. Express **13**, 2007 (2005).
[12] Z. Lu, C. Chen, C. A. Schuetz, S. Shi, J. A. Murakowski, G. J. Schneider, and D. W. Prather, Appl. Phys. Lett. **87**, 091907 (2005).
[13] C. Luo, S. G. Johnson, J. D. Joannopoulos, and J. B. Pendry, Appl. Phys. Lett. **81**, 2352 (2002).
[14] X. Ao and S. He, Opt. Lett. **29**, 2542 (2004).
[15] S. G. Johnson and J. D. Joannopoulos, Opt. Express **8**, 173 (2001).
[16] S. Foteinopoulou and C. M. Soukoulis, Phys. Rev. B **67**, 235107 (2003).
[17] In the description, we use Cartesian coordinates with the origin in the middle of the lens surface on the image side. The z axis coincides with the optical axis, whereas the x axis and y axis represent the horizontal and vertical directions, respectively. The coordinate system is also illustrated in Fig. 1(c).
[18] M. Golosovsky, Y. Neve-Oz, D. Davidov, and A. Frenkel, Phys. Rev. B **70**, 115105 (2004).
[19] The lack of surface waves in Fig. 4, which are present in the simulations of Ref. [8], reflect the limitations of our scanning setup, and, in particular, the difficulty of obtaining data very close to the surface of the photonic-crystal, where the surface evanescent waves reside; see Fig. 5(b) in Ref. [8]. However, these waves can be observed farther away from the surface for frequencies detuned from the optimum image frequency. These results will be reported elsewhere.